Available online at www.sciencedirect.com
SCIENCE DIRECT®
Finite Elements in Analysis and Design 40 (2004) 425–448
FINITE ELEMENTS IN ANALYSIS AND DESIGN
www.elsevier.com/locate/finel

Three-field mixed formulation for the non-linear analysis of composite beams with deformable shear connection

Andrea Dall'Asta[a,*], Alessandro Zona[b]

[a] *Dipartimento di Progettazione e Costruzione dell'Ambiente, University of Camerino, Viale della Rimembranza, 63100 Ascoli Piceno, Italy*

[b] *Istituto di Scienza e Tecnica delle Costruzioni, University of Ancona, Via Brecce Bianche, 60131 Ancona, Italy*

Received 25 August 2002; received in revised form 27 January 2003; accepted 9 February 2003

Abstract

A three-field mixed finite element is proposed for the non-linear analysis of composite beam with deformable shear connection. The formulation considers the non-linear behaviour of materials and shear connectors. The established mixed element is compared to the locking-free displacement element from which it derives and to a refined locking-free displacement element previously tested by the authors. In order to evaluate the way to better improve the solution in the non-linear range (three-field mixed formulation or refined displacement formulation), numerical applications are performed using, as working example, a steel-concrete cantilever, representing a difficult test for composite beam elements.

Keywords: Composite beams; Mixed formulation; Locking; Shear connection; Deformable shear connection; Non-linear analysis

1. Introduction

Composite beams are widely used in structural and bridge engineering and a beam model accounting for the non-linear behaviour of both materials and deformable shear connectors is needed for an accurate and reliable description of the deformability and the ultimate carrying load capacity. If the study is limited to the in-plane bending behaviour, i.e. symmetric cross-sections are considered and no torsion and out-of-symmetry-plane bending occur, the analysis of this type of structures can be based on the Newmark kinematical model [1]: the Kirchhoff beam theory is used to model the two parts of the composite beam; the effects of the deformable shear connection are accounted for

* Corresponding author. Tel.: +39-071-220-4551; fax: +39-071-220-4576.
E-mail address: dallasta@unian.it (A. Dall'Asta).

0168-874X/$ - see front matter © 2003 Elsevier B.V. All rights reserved.
doi:10.1016/S0168-874X(03)00071-4

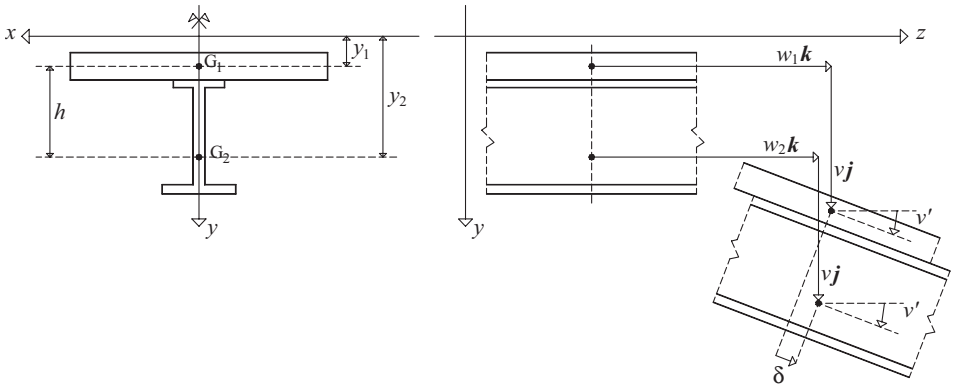

Fig. 1. Kinematical model for the composite beam with weak shear connection.

by using an interface model with distributed bond, preserving the contact between the components (Fig. 1).

Numerical solutions provided by the finite element method are very helpful in the analysis and design of this type of structures but an efficient and reliable composite beam element is required. Different displacement-based finite element models have been proposed [2–4]. Finite elements based on the displacement method have a simple formulation but their behaviour is not always satisfactory. For example the finite element satisfying the lower regularity requirements is affected by locking when shear connection stiffness increases [5]. Moreover, even if locking-free elements are adopted, a high number of DOF may be necessary in order to obtain reliable results in non-linear analysis [4].

Models that attempt to overcome the limitations of the displacement based formulations have been proposed. Salari et al. [6] and Salari et Spacone [7] adopted a finite element based on the force method (flexibility formulation), demonstrating that a more accurate calculation of the stress and strain fields, with respect to displacement based elements, is possible. However in the flexibility formulation a not straightforward iterative procedure is needed to determine the element state, as described in [8,9]. Moreover difficulties arise in selecting the force interpolation functions that strictly satisfy equilibrium for cases that involve interaction between beam displacements and internal forces, as occurs in composite beams with weak shear connection.

In view of the limitations of the displacement formulation and the difficulties of the flexibility formulation, Ayoub et Filippou [10] and Ayoub [11] introduced a displacement-stress mixed element. The mixed approach seems to combine the advantages of both displacement and force formulations, while overcoming most of their limitations. In the finite element described in [10,11] only three components of the stress field (the two axial forces and the summation of the bending moments of the two components) are described by force shape functions while the interface force is derived from the displacement field.

In this paper, the authors propose a three-field mixed element in order to evaluate its efficiency in comparison with locking free displacement elements with internal nodes tested in [4,5]. In the case of linear or non-linear elastic materials the proposed formulation is equivalent to the formulation based on the Hu-Washizu variational principle (see [12] for historical and technical details).

The displacement field of a locking-free element, the strain field (two axial deformations, curvature, interface slip) and the stress field (two axial forces, summation of the bending moments of the two components, interface shear force) are introduced and independently approximated. Since the definition of the three-field mixed element starts from a locking-free displacement field (that of the 10DOF displacement element [5]), the mixed formulation is adopted here as a stress recovery technique to enhance the stress representation [13], and not as a method to reduce or eliminate locking. Such an approach has been developed for improving the effectiveness in the non-linear range of the 10DOF element, while in the linear range the proposed mixed element has the same behaviour of the element from which it is derived, as can be deduced from the Limitation Theorems [14,15]. The established three-field mixed element is compared to the 10DOF element and to a refined locking-free displacement based element (16DOF) obtained by improving the 10DOF element with further internal nodes and previously tested by the authors [4,5]. Both the three-field element and the 16DOF displacement element require more tedious computation with respect to the 10DOF element and the comparison is developed in order to establish the better approach to use in order to overcome the problems involved in the 10DOF element.

In the sequel, the kinematical model of the composite beam with interlayer slip is described and the main equations are introduced. The finite element displacement formulation is then briefly summarized. Finally the proposed three-field approach is introduced and numerical applications are illustrated. In the examples, a steel-concrete cantilever beam is considered and uniform loads were applied downward (cracking of the concrete slab) and upward (softening of the concrete slab). The cantilever structural scheme was analysed since it is a difficult test for composite beam elements, due to high slip gradient and strain localizations. The same problems affect continuous beams (a problem of practical interest in structural engineering); the main difficulties can however be more clearly highlighted in the simpler cantilever scheme.

2. Kinematical assumptions and governing equations

2.1. Kinematical model

In the reference configuration, the composite beam occupies the cylindrical region $V = A \times [0, L]$ generated by translating its symmetrical cross-section A along a rectilinear axis, orthogonal to the cross-section. The cross-section is divided into two parts $A = A_1 \cup A_2$. We introduce an orthonormal reference frame $\{O; X, Y, Z\}$ where Z is orthogonal to A; YZ is the symmetry plane for A, A_1 and A_2; $\boldsymbol{i}$, $\boldsymbol{j}$, $\boldsymbol{k}$ are the unit vectors of axis X, Y, Z respectively. It is assumed that the connection does not permit a displacement jump in the direction orthogonal to the beam axis and only discontinuities parallel to the beam axis may occur, so that the jump condition can be expressed as follows:

$$[\boldsymbol{u}_\alpha] \cdot \boldsymbol{j} = 0, \tag{1}$$

where $\boldsymbol{u}_\alpha$ is the displacement field of part α ($\alpha = 1, 2$) with $\boldsymbol{u}_\alpha \cdot \boldsymbol{i} = 0$; this condition implies the same displacement in the Y-direction for the two beam components.

The deformed configuration is described by the following displacement field:

$$\boldsymbol{u}_\alpha(y, z) = v(z)\boldsymbol{j} + [w_\alpha(z) + (y_\alpha - y)v'(z)]\boldsymbol{k} \quad \text{on } A_\alpha \ (\alpha = 1, 2), \tag{2}$$

where the prime denotes the derivative with respect to the z co-ordinate and v, w_α are the scalar components in Y and Z directions of the displacement of the centroid of A_α located at the ordinate y_α (see Fig. 1).

2.2. Balance and compatibility conditions

The Virtual Work Principle permits obtaining compatibility and balance conditions and identifying the dynamic entities which are duals of the kinematic entities introduced by the kinematical assumptions. Such dynamic entities are resultants of the stresses which make work (active stress). The Virtual Work Principle specified for the problem in examination becomes:

$$\begin{aligned}&\sum_\alpha \int_0^L \int_{A_\alpha} \sigma_{z\alpha}\hat{\varepsilon}_{z\alpha}\,\mathrm{d}A_\alpha\,\mathrm{d}z + \int_0^L f_s\hat{\delta}\,\mathrm{d}z \\ &\quad = \sum_\alpha \int_0^L \int_{A_\alpha} \boldsymbol{b}\cdot\hat{\boldsymbol{u}}_\alpha\,\mathrm{d}A_\alpha\,\mathrm{d}z + \sum_\alpha \int_0^L \int_{\partial A_\alpha} \boldsymbol{t}\cdot\hat{\boldsymbol{u}}_\alpha\,\mathrm{d}s_\alpha\,\mathrm{d}z \qquad \forall\hat{\boldsymbol{u}}_\alpha,\end{aligned} \tag{3}$$

where $\hat{\boldsymbol{u}}_\alpha$ is the admissible displacement field, $\varepsilon_{z\alpha}$ is the axial strain given by

$$\varepsilon_{z\alpha}(y,z) = \varepsilon_\alpha(z) + (y - y_\alpha)\chi(z) \quad \text{on } A_\alpha \ (\alpha = 1,2) \tag{4}$$

($\varepsilon_\alpha = w_\alpha'$ is the axial strain evaluated at the centroid of A_α and $\chi = -v''$ is the curvature); δ is the slip between the two parts of the composite beam:

$$\delta(z) = w_2(z) - w_1(z) + hv'(z), \tag{5}$$

where $h = y_2 - y_1$ is the distance of the two components centroids (Fig. 1); $\sigma_{z\alpha}$ is the normal stress (it can be calculated from the axial strain after the introduction of the constitutive relationship for the composite beam materials); f_S is the shear connection force, assumed to be distributed along the interface (it can be calculated from the slip after having assigned the connection constitutive relationship); $\boldsymbol{b}$ and $\boldsymbol{t}$ are the body and surface forces respectively (for the sake of brevity no forces are prescribed at the end sections).

Once the stress resultants:

$$N_\alpha = \int_{A_\alpha} \sigma_{z\alpha}\,\mathrm{d}A_\alpha, \quad M_\alpha = \int_{A_\alpha} \sigma_{z\alpha}(y - y_\alpha)\,\mathrm{d}A_\alpha \tag{6a,b}$$

$M_{12} = M_1 + M_2$, and the load resultants:

$$g_{z\alpha} = \int_{A_\alpha} \boldsymbol{b}\cdot\boldsymbol{k}\,\mathrm{d}A_\alpha + \int_{\partial A_\alpha} \boldsymbol{t}\cdot\boldsymbol{k}\,\mathrm{d}s_\alpha, \tag{7a}$$

$$g_y = \sum_\alpha \int_{A_\alpha} \boldsymbol{b}\cdot\boldsymbol{j}\,\mathrm{d}A_\alpha + \sum_\alpha \int_{\partial A_\alpha} \boldsymbol{t}\cdot\boldsymbol{j}\,\mathrm{d}s_\alpha, \tag{7b}$$

$$m_x = \sum_\alpha \int_{A_\alpha} \boldsymbol{b} \cdot \boldsymbol{k}(y_\alpha - y)\,\mathrm{d}A_\alpha + \sum_\alpha \int_{\partial A_\alpha} \boldsymbol{t} \cdot \boldsymbol{k}(y_\alpha - y)\,\mathrm{d}s_\alpha \tag{7c}$$

have been introduced, the Virtual Work Principle can be expressed in the concise form:

$$\int_0^L \boldsymbol{r} \cdot \hat{\boldsymbol{\varepsilon}}\,\mathrm{d}z = \int_0^L \boldsymbol{g} \cdot \mathscr{H}\hat{\boldsymbol{u}}\,\mathrm{d}z \quad \forall[\hat{\boldsymbol{u}}, \hat{\boldsymbol{\varepsilon}}] \tag{8}$$

having introduced the displacements vector (9), the vector of generalized strains (10), the vector of stress resultants (11), the generalized load vector (12):

$$\boldsymbol{u}^{\mathrm{T}} = [w_1 \quad w_2 \quad v], \tag{9}$$

$$\boldsymbol{\varepsilon}^{\mathrm{T}} = [\varepsilon_1 \quad \varepsilon_2 \quad \chi \quad \delta], \tag{10}$$

$$\boldsymbol{r}^{\mathrm{T}} = [N_1 \quad N_2 \quad M_{12} \quad f_{\mathrm{s}}], \tag{11}$$

$$\boldsymbol{g}^{\mathrm{T}} = [g_{z1} \quad g_{z2} \quad g_y \quad m_x] \tag{12}$$

and the differential operator

$$\mathscr{H} = \begin{bmatrix} 1 & 0 & 0 \\ 0 & 1 & 0 \\ 0 & 0 & 1 \\ 0 & 0 & \partial \end{bmatrix}. \tag{13}$$

The compatibility condition is expressed by

$$\boldsymbol{\varepsilon} = \mathscr{D}\boldsymbol{u}, \tag{14}$$

where the differential operator

$$\mathscr{D} = \begin{bmatrix} \partial & 0 & 0 \\ 0 & \partial & 0 \\ 0 & 0 & -\partial^2 \\ -1 & 1 & h\partial \end{bmatrix} \tag{15}$$

permits obtaining the generalized strain vector from the displacements field (∂ denotes the derivative with respect to the z co-ordinate).

The local equilibrium conditions are obtained by integrating by parts of (8) (Euler problem) and they have the following expression:

$$\mathscr{D}^{\mathrm{T}}\boldsymbol{r} = \mathscr{H}^{\mathrm{T}}\boldsymbol{g} \tag{16}$$

(the apex T denotes the adjoint of the differential operators) while the eight boundary conditions are

$$N_\alpha(z)\hat{w}_\alpha(z)|_{z=0,L} = 0 \quad \forall \hat{w}_\alpha, \tag{17a}$$

$$M_{12}(z)\hat{v}'(z)|_{z=0,L} = 0 \quad \forall \hat{v}, \tag{17b}$$

$$(M'_{12}(z) + h f_s(z))\hat{v}(z)|_{z=0,L} = 0 \quad \forall \hat{v}. \tag{17c}$$

2.3. Constitutive law

The generalized constitutive law can be derived from the materials and shear connection constitutive laws

$$\sigma_{z\alpha} = c_\alpha(\varepsilon_{z\alpha}), \tag{18a}$$

$$f_s = c_s(\delta), \tag{18b}$$

where c_α and c_s are non-linear functions, and assumes the form

$$\boldsymbol{r} = \boldsymbol{c}(\boldsymbol{\varepsilon}). \tag{19}$$

The non-linear generalized constitutive law can be linearized referring to stress and strain increments

$$\Delta \boldsymbol{r} \cong \boldsymbol{D}_t(\boldsymbol{\varepsilon}_i)\Delta\boldsymbol{\varepsilon} \tag{20}$$

($\Delta \boldsymbol{r} = \boldsymbol{r}_{i+1} - \boldsymbol{r}_i$ and $\Delta\boldsymbol{\varepsilon} = \boldsymbol{\varepsilon}_{i+1} - \boldsymbol{\varepsilon}_i$) having introduced the symmetric operator

$$\boldsymbol{D}_t(\boldsymbol{\varepsilon}_i) = \left.\frac{\partial \boldsymbol{r}}{\partial \boldsymbol{\varepsilon}}\right|_{\varepsilon_i} = \begin{bmatrix} D_{11} & 0 & D_{13} & 0 \\ 0 & D_{22} & D_{23} & 0 \\ D_{13} & D_{23} & D_{33} & 0 \\ 0 & 0 & 0 & D_{44} \end{bmatrix}, \tag{21}$$

where

$$D_{\alpha\alpha} = \frac{\partial N_\alpha}{\partial \varepsilon_\alpha} = \int_{A_\alpha} \frac{\mathrm{d}\sigma_{z\alpha}}{\mathrm{d}\varepsilon_{z\alpha}}\,\mathrm{d}A_\alpha, \tag{22a}$$

$$D_{\alpha 3} = \frac{\partial N_\alpha}{\partial \chi} = \int_{A_\alpha} \frac{\mathrm{d}\sigma_{z\alpha}}{\mathrm{d}\varepsilon_{z\alpha}}(y - y_\alpha)\,\mathrm{d}A_\alpha, \tag{22b}$$

$$D_{33} = \sum_\alpha \frac{\partial M_\alpha}{\partial \chi} = \sum_\alpha \int_{A_\alpha} \frac{\mathrm{d}\sigma_{z\alpha}}{\mathrm{d}\varepsilon_{z\alpha}}(y - y_\alpha)^2\,\mathrm{d}A_\alpha, \tag{22c}$$

$$D_{44} = \frac{\mathrm{d}f_s}{\mathrm{d}\delta} \tag{22d}$$

since all other terms are null.

In the linear elastic case constitutive laws of materials and shear connection are linear functions

$$\sigma_{z\alpha} = E_\alpha \varepsilon_{z\alpha}, \tag{23a}$$

$$f_s = k\delta \tag{23b}$$

and the generalized linear constitutive law assumes the form

$$\boldsymbol{r} = \boldsymbol{D}\boldsymbol{\varepsilon} \tag{24}$$

having introduced the symmetric operator

$$\boldsymbol{D} = \begin{bmatrix} EA_1 & 0 & 0 & 0 \\ 0 & EA_2 & 0 & 0 \\ 0 & 0 & EJ_{12} & 0 \\ 0 & 0 & 0 & k \end{bmatrix}, \tag{25}$$

where the following quantities, containing the inertial properties of the cross-section and constitutive parameters, are introduced

$$EA_\alpha = \int_{A_\alpha} E_\alpha \, \mathrm{d}A_\alpha, \tag{26a}$$

$$EJ_\alpha = \int_{A_\alpha} E_\alpha (y - y_\alpha)^2 \, \mathrm{d}A_\alpha \tag{26b}$$

and $EJ_{12} = EJ_1 + EJ_2$ (i.e. the bending stiffness in absence of shear connection).

3. Displacement formulation

3.1. Finite element displacement formulation

The problem can be approached by assuming the displacements as unknown and using the balance condition (16), the compatibility condition (14) and the generalized constitutive law (19). The strong form of the balance condition (16) in terms of displacement is

$$\mathscr{D}^{\mathrm{T}} \boldsymbol{c}(\mathscr{D}\boldsymbol{u}) = \mathscr{H}^{\mathrm{T}} \boldsymbol{g} \tag{27}$$

while the weak form is

$$\int_0^L [\mathscr{D}^{\mathrm{T}} \boldsymbol{c}(\mathscr{D}\boldsymbol{u}) - \mathscr{H}^{\mathrm{T}} \boldsymbol{g}] \cdot \hat{\boldsymbol{u}} \, \mathrm{d}z = 0 \quad \forall \hat{\boldsymbol{u}}, \tag{28}$$

where $\hat{\boldsymbol{u}}$ is the admissible displacement field.

An approximated solution can be calculated using the displacement approach of the finite element method. The displacements formulation of the finite element method introduces a polynomial approximation of the displacement field at the interior of each element

$$\tilde{\boldsymbol{u}} = \boldsymbol{N}\boldsymbol{d}, \tag{29}$$

where $\boldsymbol{N}$ is the matrix of shape functions and $\boldsymbol{d}$ is the vector of the nodal displacements parameters (hereinafter $\tilde{\bullet}$ denotes the approximation of field $\bullet$). The strain vector $\tilde{\boldsymbol{\varepsilon}}_u$ is obtained from the

approximated displacement field

$$\tilde{\boldsymbol{\varepsilon}}_u = \mathscr{D}\boldsymbol{N}\boldsymbol{d} = \boldsymbol{B}\boldsymbol{d}. \tag{30}$$

Using constitutive laws it is possible to relate the generalized stress vector to the nodal displacement vector. The stress vector $\tilde{\boldsymbol{r}}_u$ deduced from the approximated displacement field has the expression

$$\tilde{\boldsymbol{r}}_u = \boldsymbol{c}(\tilde{\boldsymbol{\varepsilon}}_u) = \boldsymbol{c}(\boldsymbol{B}\boldsymbol{d}). \tag{31}$$

The weak form of the balance condition at element level, after substituting the approximations (29), (30) and (31), becomes

$$\int_0^{L_e} [\mathscr{D}^{\mathrm{T}}\boldsymbol{c}(\boldsymbol{B}\boldsymbol{d}) - \mathscr{H}^{\mathrm{T}}\boldsymbol{g}] \cdot \boldsymbol{N}\hat{\boldsymbol{d}}\,\mathrm{d}z = 0 \quad \forall \hat{\boldsymbol{d}} \tag{32}$$

from which the following solving balance equation is obtained:

$$\boldsymbol{f}_{r,\mathrm{PE}}(\boldsymbol{d}) - \boldsymbol{f} = \boldsymbol{0}, \tag{33}$$

where

$$\boldsymbol{f}_{r,\mathrm{PE}}(\boldsymbol{d}) = \int_0^{L_e} \boldsymbol{B}^{\mathrm{T}}\boldsymbol{c}(\boldsymbol{B}\boldsymbol{d})\,\mathrm{d}z, \tag{34}$$

$$\boldsymbol{f} = \int_0^{L_e} (\mathscr{H}\boldsymbol{N})^{\mathrm{T}}\boldsymbol{g}\,\mathrm{d}z \tag{35}$$

are the element internal forces vector and the element loads vector respectively. In the case of linear and non-linear elastic materials, the same result is obtained making stationary the functional of Total Potential Energy.

Since the equilibrium equations are non-linear an iterative method must be used. If the Newton–Raphson method is adopted then the equilibrium equation are solved using the iterative formula

$$\boldsymbol{K}_{t,\mathrm{PE}}(\boldsymbol{d}_i)(\boldsymbol{d}_{i+1} - \boldsymbol{d}_i) - (\boldsymbol{f} - \boldsymbol{f}_{r,\mathrm{PE}}(\boldsymbol{d}_i)) = \boldsymbol{0} \tag{36}$$

where

$$\boldsymbol{K}_{t,\mathrm{PE}}(\boldsymbol{d}) = \int_0^{L_e} \boldsymbol{B}^{\mathrm{T}}\boldsymbol{D}_t(\boldsymbol{B}\boldsymbol{d})\boldsymbol{B}\,\mathrm{d}z \tag{37}$$

is the element tangent stiffness matrix.

3.2. Displacement based elements

In previous works by the authors, three different displacement based elements were used and compared, with reference to linear [5] and non-linear analyses [4]. The elements considered are the 8DOF (also called PE012, the simplest element with only external nodes, linear axial displacement and cubic Hermite polynomials for transverse displacement), the 10DOF (also called PE112) and the 16DOF (also called PE334) elements (see Fig. 2 and Table 1).

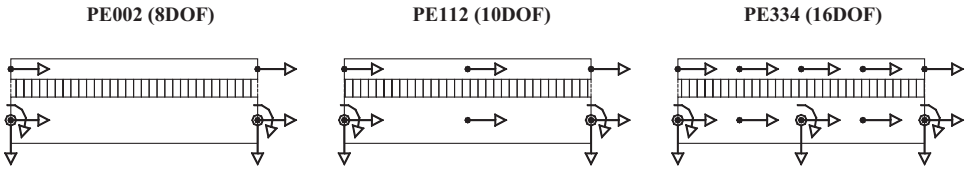

Fig. 2. Displacement fields of the 8DOF, 10DOF and 16DOF elements.

Table 1
Displacement based elements previously tested [4,5]

Element	Shape functions polynomials degree				
	Displacements		Strains		
	w	v	ε	χ	δ
PE012 (8DOF)	1	3	*0*	*1*	*2*
PE112 (10DOF)	2	3	*1*	*1*	*2*
PE334 (16DOF)	4	5	*3*	*3*	*4*

The numerical applications performed and the analytical examination of the displacement field evidenced that the 8DOF element shows locking problems and furnishes large errors for high values of the connection stiffness. This pathology can be avoided by appropriately selecting additional internal nodes in order to have both contributions to slip description, deriving from axial and transverse approximations, represented by polynomials of the same degree [5]. By starting from the 8DOF element, the problem can be surpassed by introducing an additional DOF for each of the two axial displacements, obtaining a 10DOF element with two internal nodes for w_1 and w_2. In this element, both contributions to slip description are second order polynomials.

Another element based on the choice of calibrated internal nodes is the 16DOF element, obtained from the 8DOF displacement field introducing an internal node, with one translational and one rotational DOF, for the transverse field description (v is now a fifth order Hermite polynomial), and three internal nodes for each of the two axial displacement fields. The resulting slip description is a fourth order polynomial.

However, even if locking-free displacement elements are used, a large number of elements may be required in order to obtain an accurate description of the stress and strain fields in a non-linear analysis. If, in fact, an inadequate discretization is adopted, strong irregularities in stress and strain description may arise when the beam reaches the plastic range, as illustrated in [4].

4. Three-field mixed formulation

4.1. Finite element three-field formulation

The problem can be approached by assuming the displacement, strain and stress fields as unknowns and solved using the strong formulation made by the compatibility condition (14), balance condition

(16) and the generalized constitutive law (19). The problem can also be approached using the weak form

$$\int_0^L \{[\mathscr{D}^{\mathrm{T}}\boldsymbol{r} - \mathscr{H}^{\mathrm{T}}\boldsymbol{g}] \cdot \hat{\boldsymbol{u}} + [\boldsymbol{r} - \boldsymbol{c}(\boldsymbol{\varepsilon})] \cdot \hat{\boldsymbol{\varepsilon}} + [\boldsymbol{\varepsilon} - \mathscr{D}\boldsymbol{u}] \cdot \hat{\boldsymbol{r}}\} \, \mathrm{d}z = 0 \quad \forall [\hat{\boldsymbol{u}}, \hat{\boldsymbol{\varepsilon}}, \hat{\boldsymbol{r}}], \tag{38}$$

where $[\hat{\boldsymbol{u}}, \hat{\boldsymbol{\varepsilon}}, \hat{\boldsymbol{r}}]$ are the admissible displacement, strain and stress fields.

An approximated solution can be obtained using a three-field formulation of the finite element method. The method introduces polynomial approximations of the displacement field, of the strain field and of the stress field at the interior of each element:

$$\tilde{\boldsymbol{u}} = \boldsymbol{N}\boldsymbol{d}, \tag{39a}$$

$$\tilde{\boldsymbol{\varepsilon}} = \boldsymbol{E}\boldsymbol{e}, \tag{39b}$$

$$\tilde{\boldsymbol{r}} = \boldsymbol{S}\boldsymbol{s}, \tag{39c}$$

where $\boldsymbol{N}$, $\boldsymbol{E}$ and $\boldsymbol{S}$ are the matrices of shape functions and $\boldsymbol{d}$, $\boldsymbol{e}$ and $\boldsymbol{s}$ are the vectors of nodal displacement, strain and stress parameters.

The weak form (38), after substituting the approximations (39), can be written at element level:

$$\int_0^L \{[\mathscr{D}^{\mathrm{T}}\boldsymbol{S}\boldsymbol{s} - \mathscr{H}^{\mathrm{T}}\boldsymbol{g}] \cdot \boldsymbol{N}\hat{\boldsymbol{d}} + [\boldsymbol{S}\boldsymbol{s} - \boldsymbol{c}(\boldsymbol{E}\boldsymbol{e})] \cdot \boldsymbol{E}\hat{\boldsymbol{e}} + [\boldsymbol{E}\boldsymbol{e} - \boldsymbol{B}\boldsymbol{d}] \cdot \boldsymbol{S}\hat{\boldsymbol{s}}\} \, \mathrm{d}z = 0 \quad \forall [\hat{\boldsymbol{d}}, \hat{\boldsymbol{e}}, \hat{\boldsymbol{s}}] \tag{40}$$

and the following solving equations can be obtained

$$\bar{\boldsymbol{B}}^{\mathrm{T}}\boldsymbol{s} - \boldsymbol{f} = \boldsymbol{0}, \tag{41a}$$

$$\boldsymbol{a}(\boldsymbol{e}) - \bar{\boldsymbol{E}}^{\mathrm{T}}\boldsymbol{s} = \boldsymbol{0}, \tag{41b}$$

$$\bar{\boldsymbol{E}}\boldsymbol{e} - \bar{\boldsymbol{B}}\boldsymbol{d} = \boldsymbol{0}, \tag{41c}$$

where

$$\bar{\boldsymbol{B}} = \int_0^{L_e} \boldsymbol{S}^{\mathrm{T}}\boldsymbol{B} \, \mathrm{d}z, \tag{42}$$

$$\bar{\boldsymbol{E}} = \int_0^{L_e} \boldsymbol{S}^{\mathrm{T}}\boldsymbol{E} \, \mathrm{d}z, \tag{43}$$

$$\boldsymbol{a}(\boldsymbol{e}) = \int_0^{L_e} \boldsymbol{E}^{\mathrm{T}}\boldsymbol{c}(\boldsymbol{E}\boldsymbol{e}) \, \mathrm{d}z. \tag{44}$$

Note that the equations of compatibility and equilibrium are linear, since the non-linear constitutive law does not involve the relation between displacement and strain and between stress and applied loads. In the case of linear or non-linear elastic materials, the same system (41) is obtained making stationary the Hu-Washizu variational principle.

The non-linear problem can be solved using an iterative method. If the Newton–Raphson method is adopted then the problem is solved using the iterative formulas

$$\bar{\boldsymbol{D}}_t(\boldsymbol{e}_i)(\boldsymbol{e}_{i+1}-\boldsymbol{e}_i)-(\bar{\boldsymbol{E}}^{\mathrm{T}}\boldsymbol{s}-\boldsymbol{a}(\boldsymbol{e}_i))=\boldsymbol{0}, \tag{45}$$

$$\bar{\boldsymbol{E}}(\boldsymbol{e}_{i+1}-\boldsymbol{e}_i)-\bar{\boldsymbol{B}}(\boldsymbol{d}_{i+1}-\boldsymbol{d}_i)=\boldsymbol{0}, \tag{46}$$

$$\bar{\boldsymbol{B}}^{\mathrm{T}}\boldsymbol{s}-\boldsymbol{f}=\boldsymbol{0}, \tag{47}$$

where

$$\bar{\boldsymbol{D}}_t(\boldsymbol{e})=\int_0^{L_e}\boldsymbol{E}^{\mathrm{T}}\boldsymbol{D}_t(\boldsymbol{E}\boldsymbol{e})\boldsymbol{E}\,\mathrm{d}z. \tag{48}$$

4.2. Condensation of the strain and force degrees of freedom

Since the stress and strain fields can be inter element discontinuous, the system of equations (45)–(47) will be simplified in the following, performing a static condensation of stress and strain nodal parameters.

The deformation nodal parameters are calculated from Eq. (45)

$$\boldsymbol{e}_{i+1}-\boldsymbol{e}_i=[\bar{\boldsymbol{D}}_t(\boldsymbol{e}_i)]^{-1}[\bar{\boldsymbol{E}}^{\mathrm{T}}\boldsymbol{s}-\boldsymbol{a}(\boldsymbol{e}_i)] \tag{49}$$

(see Appendix B in [15] for the conditions under which the matrices (48) and (51) are invertible assuming that (21) is not singular) and substituted in Eq. (46) thus obtaining

$$\bar{\boldsymbol{E}}[\bar{\boldsymbol{D}}_t(\boldsymbol{e}_i)]^{-1}\bar{\boldsymbol{E}}^{\mathrm{T}}\boldsymbol{s}-\bar{\boldsymbol{E}}[\bar{\boldsymbol{D}}_t(\boldsymbol{e}_i)]^{-1}\boldsymbol{a}(\boldsymbol{e}_i)-\bar{\boldsymbol{B}}(\boldsymbol{d}_{i+1}-\boldsymbol{d}_i)=\boldsymbol{0}. \tag{50}$$

After introducing the matrix

$$\bar{\bar{\boldsymbol{D}}}(\boldsymbol{e})=\bar{\boldsymbol{E}}[\bar{\boldsymbol{D}}_t(\boldsymbol{e})]^{-1}\bar{\boldsymbol{E}}^{\mathrm{T}} \tag{51}$$

from the previous equation the stress parameters are obtained

$$\boldsymbol{s}=[\bar{\bar{\boldsymbol{D}}}_t(\boldsymbol{e}_i)]^{-1}\{\bar{\boldsymbol{E}}[\bar{\boldsymbol{D}}_t(\boldsymbol{e}_i)]^{-1}\boldsymbol{a}(\boldsymbol{e}_i)+\bar{\boldsymbol{B}}(\boldsymbol{d}_{i+1}-\boldsymbol{d}_i)\} \tag{52}$$

and are substituted in the equation of equilibrium

$$\bar{\boldsymbol{B}}^{\mathrm{T}}[\bar{\bar{\boldsymbol{D}}}_t(\boldsymbol{e}_i)]^{-1}\bar{\boldsymbol{B}}(\boldsymbol{d}_{i+1}-\boldsymbol{d}_i)=\boldsymbol{f}-\bar{\boldsymbol{B}}^{\mathrm{T}}[\bar{\bar{\boldsymbol{D}}}_t(\boldsymbol{e}_i)]^{-1}\bar{\boldsymbol{E}}[\bar{\boldsymbol{D}}_t(\boldsymbol{e}_i)]^{-1}\boldsymbol{a}(\boldsymbol{e}_i) \tag{53}$$

or with a different notation:

$$\boldsymbol{K}_{t,\mathrm{HW}}(\boldsymbol{e}_i)(\boldsymbol{d}_{i+1}-\boldsymbol{d}_i)-(\boldsymbol{f}-\boldsymbol{f}_{r,\mathrm{HW}}(\boldsymbol{e}_i))=\boldsymbol{0}, \tag{54}$$

where

$$\boldsymbol{K}_{t,\mathrm{HW}}(\boldsymbol{e})=\bar{\boldsymbol{B}}^{\mathrm{T}}[\bar{\bar{\boldsymbol{D}}}_t(\boldsymbol{e})]^{-1}\bar{\boldsymbol{B}}, \tag{55}$$

$$\boldsymbol{f}_{r,\mathrm{HW}}(\boldsymbol{e})=\bar{\boldsymbol{B}}^{\mathrm{T}}[\bar{\bar{\boldsymbol{D}}}_t(\boldsymbol{e})]^{-1}\bar{\boldsymbol{E}}[\bar{\boldsymbol{D}}_t(\boldsymbol{e})]^{-1}\boldsymbol{a}(\boldsymbol{e}) \tag{56}$$

are the element displacement-strain tangent stiffness matrix and internal force vector, respectively.

Observe that the formulas obtained are similar to those of the finite element displacement formulation and can be easily used in a displacement based program.

5. The proposed three-field mixed element

5.1. Element formulation

Starting from an assigned displacement field, different choices can be made to represent the strain and stress fields at the interior of each element. In the linear elastic case, a proper definition of the shape functions for the three fields requires particular attention due to the Limitation Theorems [14,15]. If certain relationships between the displacement, strain and stress fields are satisfied, then the three-field mixed approach becomes identical to a two-field mixed approach, with the same displacement and stress fields, or can even become identical to a displacement-based element with the same displacement field (details in [14,15]). However, in the non-linear case, the Limitation Theorems are not effective, and more possibilities are available.

The mixed element proposed by the authors in this paper is based on the displacement field of the locking-free 10DOF element (quadratic polynomials for the axial displacements, third order Hermite polynomial for the transverse displacement). The strain field has linear shape functions for the two axial strains and curvature, while the slip shape functions are second order polynomials. The same representation is used for the stress field (linear axial forces and bending moment, second order interface force). The proposed element will be indicated hereafter as HW112, where the three digits indicate the polynomial degree of the axial, bending and interface shape functions respectively, used for both stress and strain.

The HW112 shape functions are collected in the following matrices:

$$\boldsymbol{N}_{\mathrm{HW112}} = \begin{bmatrix} \mu_{21} & 0 & 0 & 0 & \mu_{23} & 0 & \mu_{22} & 0 & 0 & 0 \\ 0 & \mu_{21} & 0 & 0 & 0 & \mu_{23} & 0 & \mu_{22} & 0 & 0 \\ 0 & 0 & \eta_1 & \eta_2 & 0 & 0 & 0 & 0 & \eta_3 & \eta_4 \end{bmatrix}, \tag{57a}$$

$$\boldsymbol{E}_{\mathrm{HW112}} = \begin{bmatrix} \mu_1 & \mu_2 & 0 & 0 & 0 & 0 & 0 & 0 & 0 \\ 0 & 0 & \mu_1 & \mu_2 & 0 & 0 & 0 & 0 & 0 \\ 0 & 0 & 0 & 0 & \mu_1 & \mu_2 & 0 & 0 & 0 \\ 0 & 0 & 0 & 0 & 0 & 0 & \mu_{21} & \mu_{22} & \mu_{23} \end{bmatrix}, \tag{57b}$$

$$\boldsymbol{S}_{\mathrm{HW112}} = \begin{bmatrix} \mu_1 & \mu_2 & 0 & 0 & 0 & 0 & 0 & 0 & 0 \\ 0 & 0 & \mu_1 & \mu_2 & 0 & 0 & 0 & 0 & 0 \\ 0 & 0 & 0 & 0 & \mu_1 & \mu_2 & 0 & 0 & 0 \\ 0 & 0 & 0 & 0 & 0 & 0 & \mu_{21} & \mu_{22} & \mu_{23} \end{bmatrix}, \tag{57c}$$

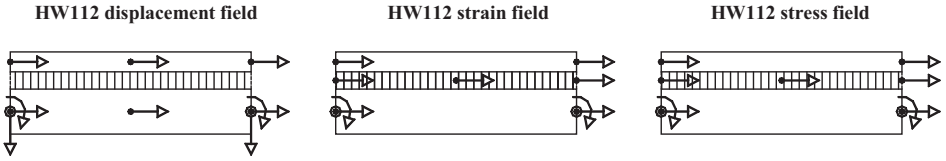

Fig. 3. Displacement, strain and stress fields of the HW112 element.

where the nodal parameters vectors are

$$\boldsymbol{d}^{\mathrm{T}}_{\mathrm{HW112}} = [w_{1A} \quad w_{2A} \quad v_A \quad \varphi_A \quad w_{1C} \quad w_{2C} \quad w_{1B} \quad w_{2B} \quad v_B \quad \varphi_B], \tag{58a}$$

$$\boldsymbol{e}^{\mathrm{T}}_{\mathrm{HW112}} = [\varepsilon_{1A} \quad \varepsilon_{1B} \quad \varepsilon_{2A} \quad \varepsilon_{2B} \quad \chi_A \quad \chi_B \quad \delta_A \quad \delta_B \quad \delta_C], \tag{58b}$$

$$\boldsymbol{s}^{\mathrm{T}}_{\mathrm{HW112}} = [N_{1A} \quad N_{1B} \quad N_{2A} \quad N_{2B} \quad M_{12A} \quad M_{12B} \quad \mathrm{f}_{SA} \quad \mathrm{f}_{SB} \quad \mathrm{f}_{SC}], \tag{58c}$$

(letters A and B refer to the end nodes at $z = 0$ and $z = L_e$, respectively, C indicates the internal node at $z = L_e/2$, see Fig. 3) and the shape functions:

$$\mu_1(z) = \tfrac{1}{2}(1 + \xi), \tag{59a}$$

$$\mu_2(z) = \tfrac{1}{2}(1 + \xi), \tag{59b}$$

$$\mu_{21}(z) = \tfrac{1}{2}(\xi^2 - \xi), \tag{59c}$$

$$\mu_{22}(z) = \tfrac{1}{2}(\xi^2 + \xi), \tag{59d}$$

$$\mu_{23}(z) = 1 - \xi^2, \tag{59e}$$

$$\eta_1(z) = \tfrac{1}{4}(2 - 3\xi + \xi^3), \tag{59f}$$

$$\eta_2(z) = \frac{L_e}{8}(1 - \xi - \xi^2 + \xi^3), \tag{59g}$$

$$\eta_3(z) = \tfrac{1}{4}(2 + 3\xi - \xi^3), \tag{59h}$$

$$\eta_4(z) = \frac{L_e}{8}(-1 - \xi + \xi^2 - \xi^3), \tag{59i}$$

with $\xi = 2z/L_e - 1$, $\xi \in [-1, 1]$, $z \in [0, L_e]$.

This element satisfies the Third Limitation Principle [15], i.e. in the linear elastic case it performs like the 10DOF element, while improvements in stress calculations are expected in the non-linear case. Note that the authors start from a locking-free displacement element, thus the mixed formulation is used only as a stress recovery technique to enhance the stress representation, and not as a method to reduce or eliminate locking.

Table 2
Displacement and mixed elements compared

Element	Shape functions polynomials degree							
	Displacements		Strains			Stresses		
	w	v	ε	χ	δ	N	M	f_s
PE112	2	3	*1*	*1*	*2*	*N.L.*	*N.L.*	*N.L.*
PE334	4	5	*3*	*3*	*4*	*N.L.*	*N.L.*	*N.L.*
HW112	2	3	1	1	2	1	1	2
HW111	2	3	1	1	1	1	1	1
HW222	2	3	2	2	2	2	2	2

Starting again from the 10DOF displacement field, other mixed elements, with richer and poorer stress and strain fields (HW222 with second order stress and strain shape functions polynomials and HW111 with linear stress and strain shape functions), were tested, but the best results were obtained from the previously described HW112 element. The three mixed elements fulfil the conditions under which the matrices (48) and (51) are invertible when matrix (21) is not singular (Appendix B in [15]); in fact the matrices $\boldsymbol{E}$ and $\boldsymbol{S}$ are identical and the number of strain nodal parameters equals the number of stress nodal parameters.

In Table 2, the degrees of the polynomials of the shape functions of HW112, HW111, HW222, PE112 and PE334 are compared. The strain and stress polynomial degree of displacement-based elements are indicated in italics because they are not independent from the displacement shape functions: the strain shape functions are derived from the displacement field by means of compatibility conditions while the stress field is non-linear since the constitutive law is non-linear.

5.2. Numerical details

The element stiffness matrix (55) and the internal force vector (56) are obtained integrating the matrices (42,43) in closed form, while the calculation of matrix (48) and vector (44) is performed by means of numerical integration, using the trapezoidal rule through the thickness (the cross-section is subdivided into rectangular strips parallel to the x-axis) and by using the Gauss-Lobatto rule [16] with 5 integration points, along the element length. Note that the matrices (42,43) are calculated only once at the beginning of the analysis, while only matrix (48) and vector (44) need to be updated during the non-linear solution procedure. Once the solution is obtained, the proposed mixed approach permits a simple calculation of stress and strains nodal parameters, allowing a prompt determination of the stress and strain fields, by means of the shape functions (39b) and (39c).

6. Applications

Some of the numerical applications performed are illustrated and discussed hereafter in order to compare the PE112 element (the simpler locking-free displacement element) with the HW112 and

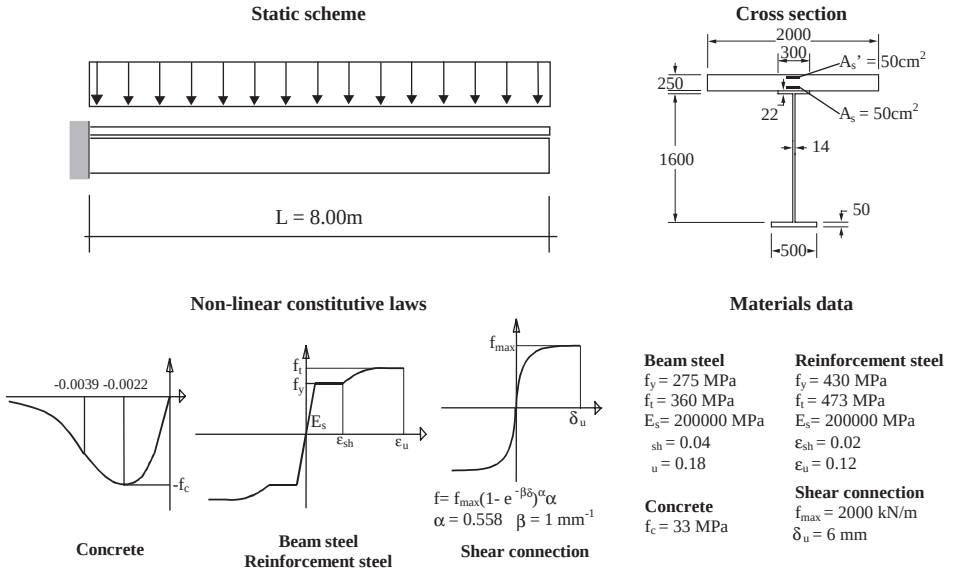

Fig. 4. Problem tested with data of the materials and non-linear constitutive laws.

PE334 elements for evaluating the better way to improve the solution (three-field mixed formulation or refined displacement formulation).

The geometry of the test problem is described in Fig. 4 (a cantilever with constant cross-section along the beam axis). Two load conditions are considered: a uniform load applied downward (cracking of the concrete slab) and a uniform load acting upward (softening of the concrete slab). With regard to the shear connection device, for the sake of simplicity a uniform distribution of stud connectors, designed to obtain a full shear connection, is adopted (i.e. the shear connection is designed not to collapse before the reinforced concrete slab and/or steel beam reach their ultimate state). The cantilever structural scheme was analysed since it is a difficult test for composite beam elements, due to the high slip gradient and strain localizations. The same problems affect continuous beams (a problem of practical interest in structural engineering), although the main difficulties can be more clearly highlighted in the simpler cantilever scheme.

The non-linear constitutive laws adopted for materials and shear connectors are the following. Elastic—perfect plastic—hardening constitutive laws are assumed for beam steel and reinforcements bars [17]; the non-linear law suggested by the CEB-FIP Model Code 1990 [18] is considered for concrete under compression while, for the sake of simplicity, null strength is used under traction; furthermore, the Ollgaard constitutive law [19] is adopted for the shear connection. The mechanical characteristics of the materials are reported in Fig. 4.

The solution of the algebraic non-linear problem obtained assembling the composite beam elements, is attained by a displacement control incremental procedure [20] whose prediction is corrected by the Newton–Raphson iterative procedure (predictor–corrector scheme, see [4] for more details and other solution procedures tested). The non-linear analyses, performed controlling the free-edge deflection, were stopped when the ultimate strain of one of the materials is achieved. When load levels near collapse were reached, the HW112 element provided a slower convergence rate than

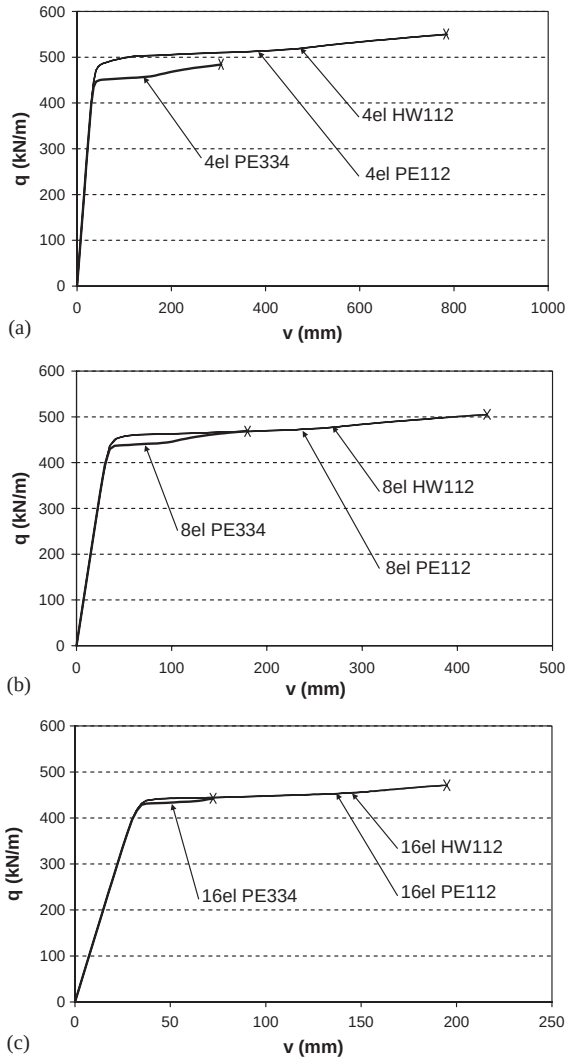

Fig. 5. (a–c) Load-deflection curves with different types and numbers of elements.

displacement based elements and smaller increments of the controlled displacement were needed to accomplish the assigned tolerance of the unbalance force vector.

The case of uniform load applied downwards is firstly considered. The structural global response is illustrated in Fig. 5, where the load-displacement curves, obtained with different elements number and type, are reported. The solutions achieved with a four-element mesh are compared in Fig. 5a, while eight and sixteen elements mesh solutions are illustrated in Figs. 5b and c, respectively. The HW112 mixed element and the PE112 displacement element practically supply the same results (see also Table 3), while the PE334 element gives lower values of collapse load and ultimate deflection, even if discretizations with the same total displacement DOF are considered (the PE334 has a more accurate approximation of the strain peaks).

Table 3
Ultimate loads and deflections using different types and number of elements

Element	Number of elements	Total displacement DOF	Ultimate load (kN/m)	Ultimate deflection (mm)
PE112	4	24	550.00	786
	8	48	505.00	431
	16	96	470.40	193
HW112	4	24	549.60	781
	8	48	505.00	430
	16	96	471.20	195
PE334	4	48	484.00	306
	8	96	469.60	180
	16	192	443.40	75

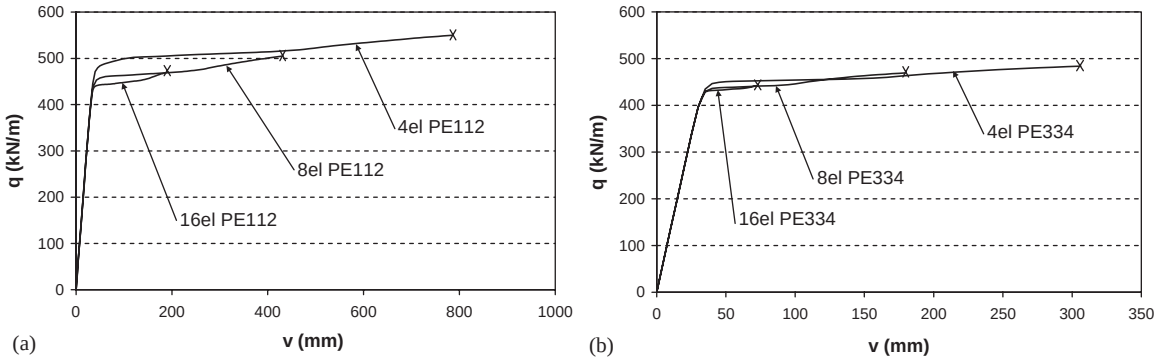

Fig. 6. (a,b) Load-displacement curves with different numbers of elements.

In Fig. 6, the load-displacement curves calculated with the same element type are considered: in Fig. 6a the three curves are obtained using the PE112 and the HW112 elements (equivalent global results), while the three curves in Fig. 6b are those obtained with the PE334 element. Note that the PE334 gives a smaller error in the ultimate load level, even if a coarse mesh is adopted.

In Figs. 7–9 the stress resultant trends along the beam axis are reported for three steps: 15 mm of free-edge deflection (dotted lines) when the steels are in the elastic range and the concrete slab cracked; 30 mm of deflection (dashed lines) when the beam and reinforcements steels are yielded and 60 mm of deflection when the plastic deformations of the steels have reached the near hardening point (for the corresponding load levels see Table 4). The steel beam axial force N_s is normalized with respect to the steel beam plastic force N_{spl} (i.e. the yielding stress multiplied by the steel beam cross-section area); the summation of steel beam bending moment and concrete slab bending moment M_{sc} is normalized with respect to the steel beam plastic moment M_{spl}; finally the interface shear force

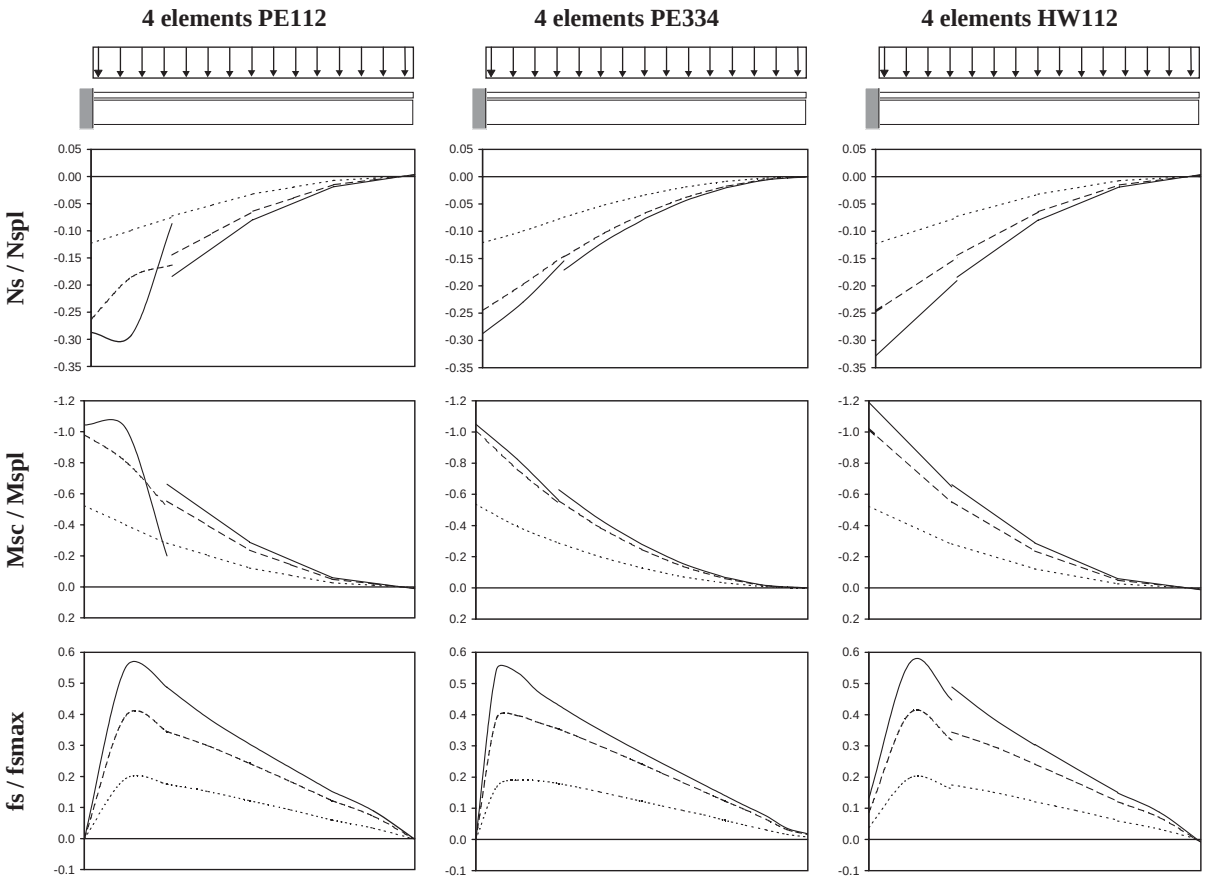

Fig. 7. Stress trends computed by a uniform mesh of 4 elements.

f_s is normalized with respect to the connection strength f_{smax}. The axial force and bending moment are inter-elements discontinuous in the displacement based elements while the interface shear force is inter-element continuous as calculated from a continuous slip (the displacements of Eq. (5) are assembled in the solving system and the distance h between the two beam components centroids is constant along the beam axis). The mixed element gives inter-elements discontinuities in both axial, bending and interface shear force, due to the static condensation of the strain and stress DOF; this results in a non compatible trend of the interface shear force (i.e. the shear force must be zero at the constrain since here the slip is zero).

In Fig. 7 the stress trends, obtained with the three types of elements from a uniform four-element mesh, are compared. Despite the global behaviour is practically the same, the PE112 element and the HW112 element perform in a different manner if the stress resultants are observed. Strong irregularities in axial force and bending moment arise in the PE112 when the load level increases, while the HW112 furnishes a smooth description of axial force and bending moment, whenever low or high load levels are considered. The PE334 displacement element is affected by some irregularities

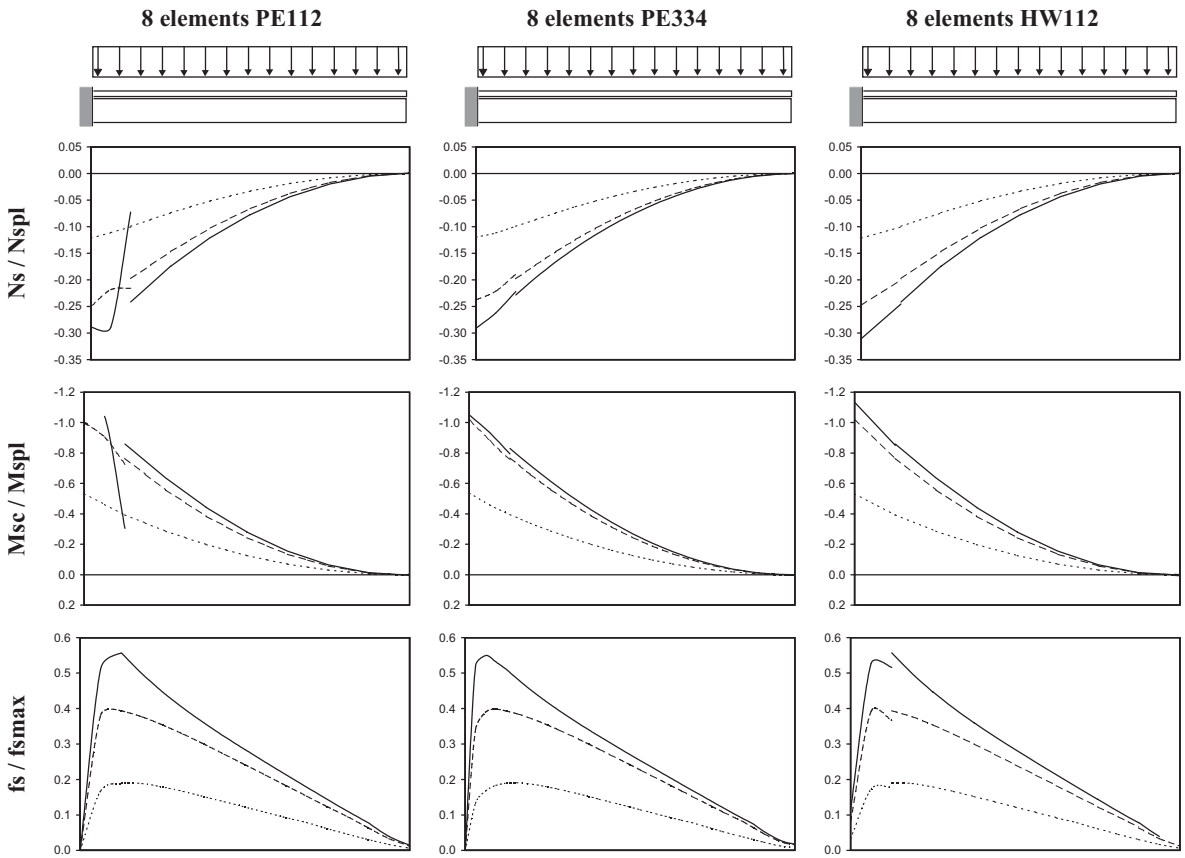

Fig. 8. Stress trends computed by a uniform mesh of 8 elements.

in the axial force and bending moment description for high load levels, while the shear force description is closer to the reference solution (sixteen PE334 elements reported in Fig. 9) compared with the other two elements; the PE334 is however based on richer displacement shape functions and the comparisons are made between solutions with different total DOF.

In Figs. 8 and 9 the same stress resultants trends are reported with reference to a uniform eight-element mesh and a uniform sixteen-element mesh, respectively. It is interesting to note that a refined mesh does not eliminate the previously described problems. In fact the irregularities in the axial force and bending moment computed by the PE112 element are still evident. The HW112 furnishes the smoother description of N_s and M_{sc}, but the interface shear force presents the same irregularities analysed in the four element discretization, although a solution closer to the reference solution is obtained by means of the increment of the number of elements.

The strain trends are not reported here for the sake of brevity. However the strain field obtained from the PE112 and PE334 elements present problems (see [4] for details) analogous to those illustrated in the stress field, while the mixed element gives the same results of the PE112 element, since the relation between displacement and strain is still linear. Consequently the proposed mixed

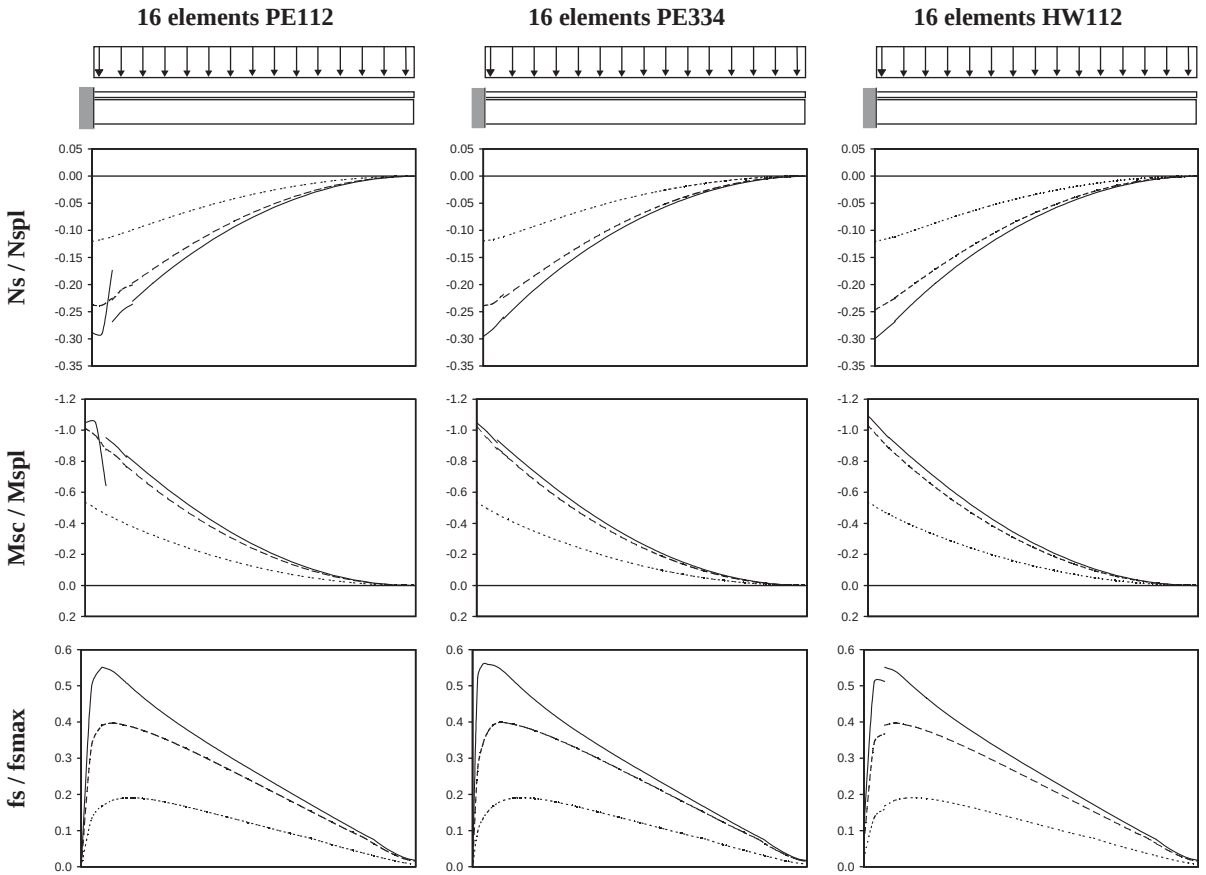

Fig. 9. Stress trends computed by a uniform mesh of 16 elements.

element permits a smoother description of axial force and bending moment than the equivalent displacement element PE112, while the other results (global behaviour, strain and displacement) are practically equivalent. Notice furthermore that the interface slip, even if it is not assembled since it is condensed out, is equal to the slip computed from the displacement field. Hence, if the interface shear force is computed from the displacement field or from the strain field, the results obtained are the same as those of the PE112 element.

In Figs. 10 and 11 some results regarding the cantilever under negative load (i.e. load applied upwards) are reported. In this load case the slab is under compression and softening of concrete occurs under high deformations. In Fig. 10 the load-displacement curves are reported: in Fig. 10a the three curves are obtained using the PE112 and the HW112 elements (once again equivalent global results), while the three curves in Fig. 10b are those obtained with the PE334 element. Note once more that the PE334 gives a smaller error in the ultimate load level, even if a coarse mesh is adopted. In Fig. 11 the stress trends, obtained with the three types of elements from a uniform four-element mesh, are compared. The stress resultants trends along the beam axis are reported for

Table 4
Compared solutions

Element	Number of elements	Deflection 15 mm Load (kN/m)	Deflection 30 mm Load (kN/m)	Deflection 60 mm Load (kN/m)
PE112	4	202.37	398.46	488.30
	8	202.36	396.99	460.20
	16	202.36	396.80	443.51
HW112	4	202.37	398.46	488.30
	8	202.36	396.99	460.20
	16	202.36	396.80	443.51
PE334	4	202.36	396.23	451.60
	8	202.36	396.60	439.41
	16	202.36	396.29	435.53

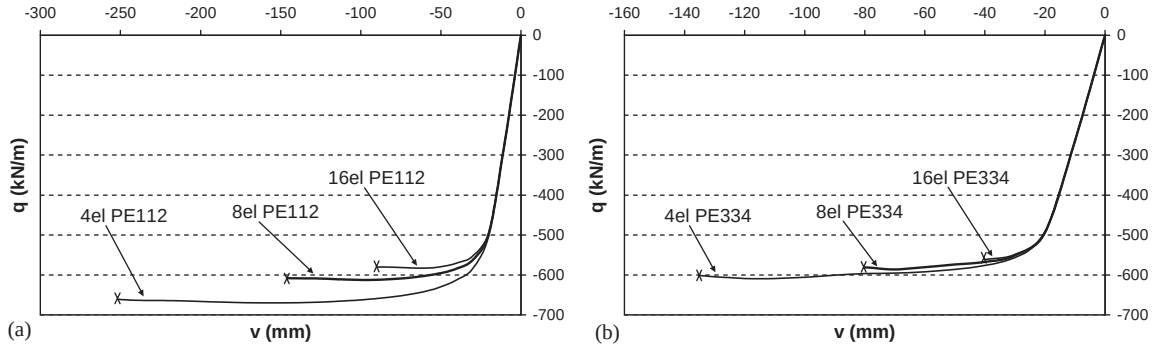

Fig. 10. (a,b) Load-displacement curves with different numbers of elements (negative load case).

three steps: 10 mm of free-edge deflection (dotted lines) when the steels are in the elastic range; 20 mm of deflection (dashed lines) when the steel beam is yielded and 40 mm of deflection when the reinforcement steel is also yielded and the concrete undergoes softening. The same considerations made in the previous case can be repeated here. In effect the axial force N_s and bending moment M_{sc} trends are quite similar to those of Fig. 7, apart from the sign. The different trend of the interface shear force f_s is due to the more complex behaviour of the reinforced concrete slab under compression.

In the previous figures only the HW112 element is analysed between mixed elements since it provides the best results with respect to the other three-field elements tested. However, for the sake of completeness, the different mixed elements are compared in Fig. 12. If the HW111 element is adopted, the descriptions of the axial force and bending moment are practically equal to those of the HW112 element, but the description of the interfacial shear force is too poor (piecewise linear). If the HW222 element is used, despite the higher degree of shape functions in the axial force and bending moment, the element provides, in these stress resultants, worse results than the HW112 element.

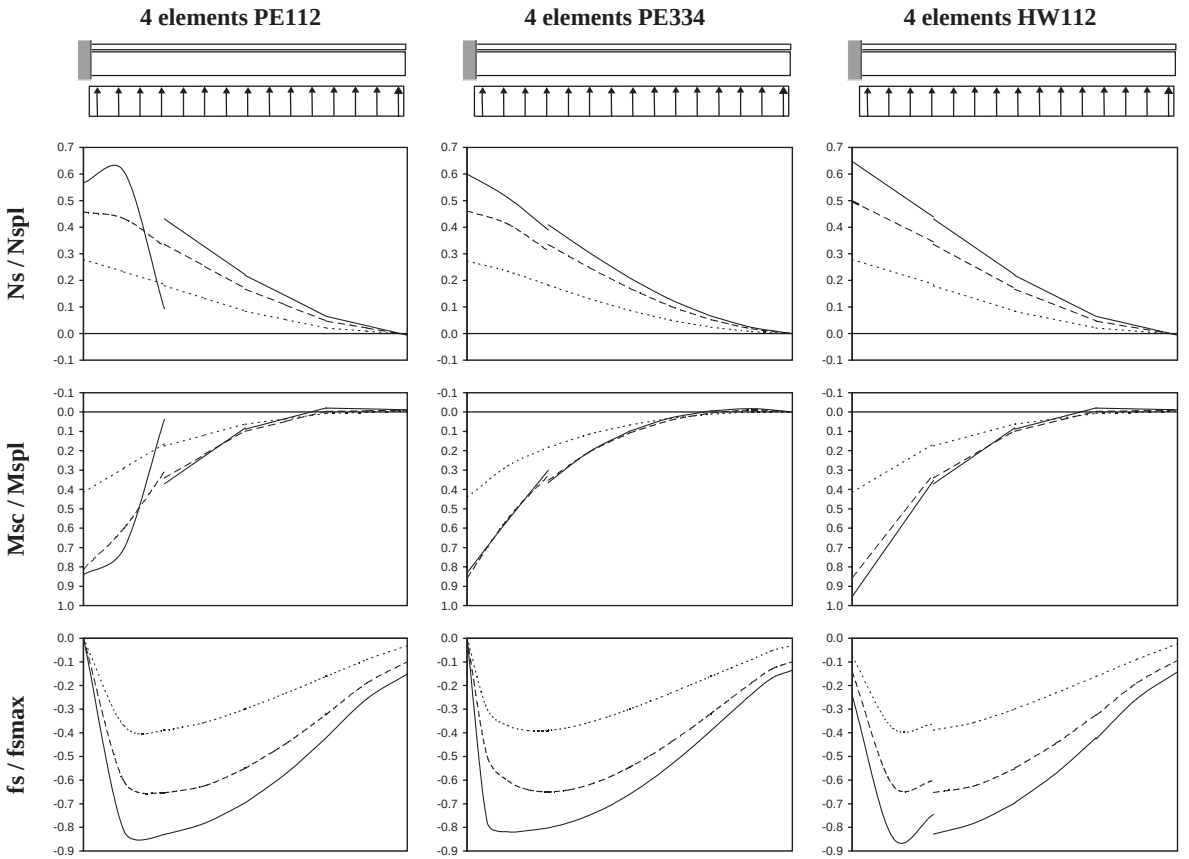

Fig. 11. Stress trends computed by a uniform mesh of 4 elements (negative load case).

7. Conclusions

A three-field mixed finite element for the non-linear analysis of composite beam with weak shear connection is proposed. The formulation considers the non-linear behaviour of materials and deformable shear connectors. The proposed element is compared with the two locking-free displacement elements previously used by the authors. In the applications a steel-concrete cantilever beam is considered and uniform loads were applied downward (cracking of the concrete slab) and upward (softening of the concrete slab). The cantilever structural scheme was analysed since it is a difficult test for composite beam elements, due to high slip gradient and strain localizations. The same troubles affect continuous beams (a problem of practical interest in structural engineering), however the main difficulties can be more clearly highlighted in the simpler cantilever scheme. The non-linear analyses performed show that the established mixed element furnishes more regular distributions of axial forces and bending moment with respect to the locking-free 10DOF displacement element from which it is derived. However the mixed element requires a more cumbersome formulation, longer computational times and has a slower convergence for high non-linearity. If the

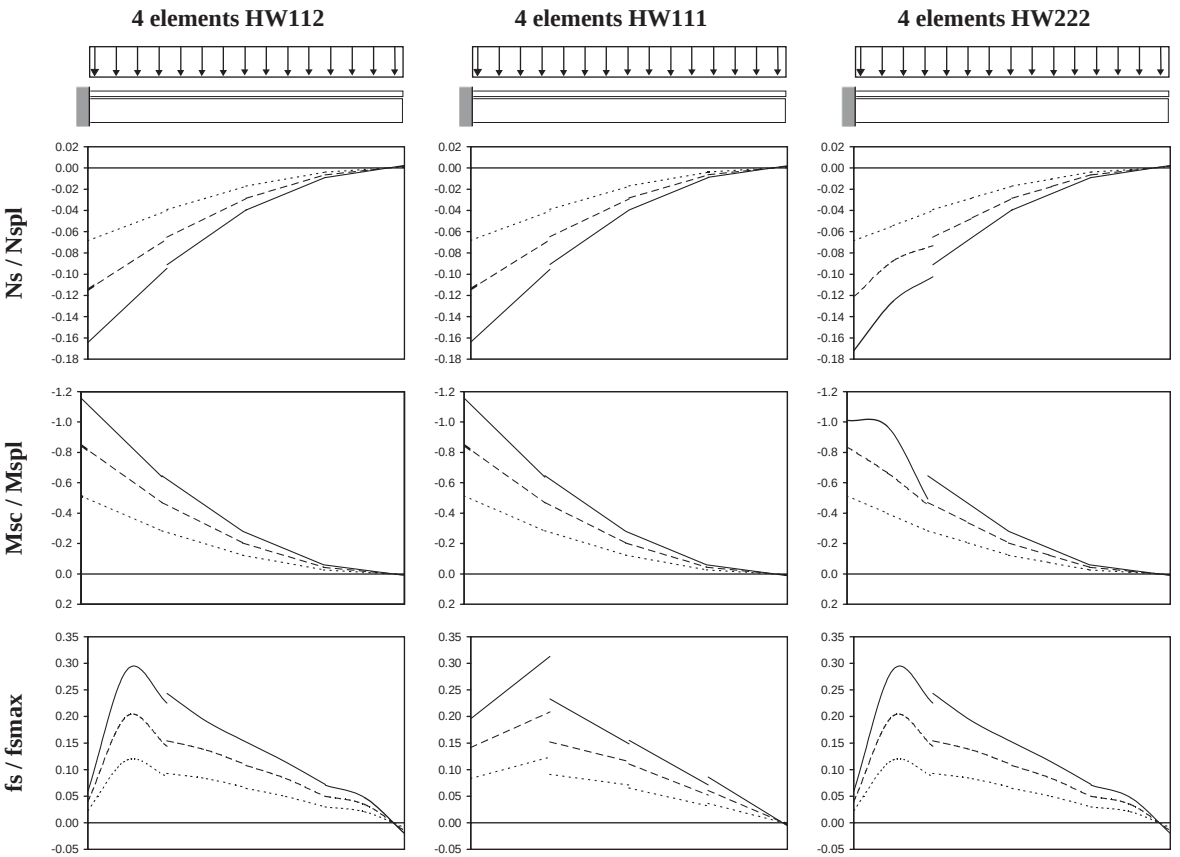

Fig. 12. Stress trends computed by a uniform mesh of 4 elements (mixed elements).

mixed element is compared to the refined locking-free 16DOF displacement element, only slight advantages are obtained with the mixed formulation in the description of axial forces and bending moment distributions, while the refined displacement element gives a more accurate description of the interface slip and the shear force, has a simpler formulation and convergence in the non-linear range is achieved with good reliability.

References

[1] N.M. Newmark, C.P. Siess, I.M. Viest, Tests and analysis of composite beams with incomplete interaction, Proc. Soc. Exp. Stress Anal. 9 (1) (1951) 75–92.

[2] Y. Arizumi, S. Hamada, T. Kajita, Elastic-plastic analysis of composite beams with incomplete interaction by finite element method, Comput. Struct. 14 (5) (1981) 453–462.

[3] B.J. Daniels, M. Crisinel, Composite slab behaviour and strength analysis. Part. I: calculation procedure, J. Struct. Eng. ASCE 119 (1) (1993) 16–35.

[4] A. Dall'Asta, A. Zona, Non-linear analysis of composite beams by a displacement approach, Comput. Struct. 80 (27–30) (2002) 2217–2228.

[5] A. Dall'Asta, A. Zona, Locking in composite beams with weak shear connection, Technical Note no. 264, Istituto di Scienza e Tecnica delle Costruzioni, University of Ancona, Italy, 2001.
[6] M.R. Salari, E. Spacone, P.B. Shing, D.M. Frangopol, Non-linear analysis of composite beams with deformable shear connectors, J. Struct. Eng. ASCE 124 (10) (1998) 1148–1158.
[7] M.R. Salari, E. Spacone, Finite element formulations of one-dimensional elements with bond-slip, Eng. Struct. 23 (7) (2001) 815–826.
[8] E. Spacone, V. Ciampi, F.C. Filippou, Mixed formulation of nonlinear beam finite element, Comput. Struct. 58 (1) (1996) 71–83.
[9] E. Spacone, F.C. Filippou, F.F. Taucer, Fibre beam-column model for non-linear analysis of r/c frames: Part I. Formulation, Earthquake Eng. Struct. Dyn. 25 (7) (1996) 711–725.
[10] A. Ayoub, F.C. Filippou, Mixed formulation of nonlinear steel-concrete composite beam element, J. Struct. Eng. ASCE 126 (3) (2000) 371–381.
[11] A. Ayoub, A two-field mixed variational principle for partially connected composite beams, Finite Elements in Analysis and Design 37 (2001) 929–959.
[12] C.A. Felippa, On the original publication of the general canonical functional of linear elasticity, J. Appl. Mech. 67 (1) (2000) 217–219.
[13] A. Mota, J.F. Abel, On mixed finite element formulation and stress recovery techniques, Int. J. Numer. Meth. Eng. 47 (1–3) (2000) 191–204.
[14] B.M. Fraeijs De Veubeke, Displacement and equilibrium models in the finite element method, in: O.C. Zienkiewicz, G.S. Hollister (Eds.), Stress Analysis, John Wiley & Sons, London, 1965, pp. 145–196 (Reprinted in Int. J. Numer. Meth. Eng. 52 (2001) 287–342).
[15] H. Stolarski, T. Belytschko, Limitation Principles for mixed finite elements based on the Hu-Washizu variational formulation, Comput. Methods Appl. Mech. Eng. 60 (1987) 195–216.
[16] M.A. Crisfield, Non-linear Finite Element Analysis of Solids and Structures, Vol. 1, Essentials, Vol. 1, Wiley, New York, 1991.
[17] FIB, Ductility of Reinforced Concrete Structures, CEB Bulletin d'Information no. 242, FIB Fédération International du Béton, Paris, France, 1998, pp. 112–113.
[18] CEB-FIP, Model Code 1990, CEB Bulletin d'Information no. 190, CEB-FIP Comité Euro-International du Béton, Paris, France, 1988.
[19] J.G. Ollgaard, R.G. Slutter, J.W. Fisher, Shear strength of stud connectors in lightweight and normal weight concrete, Eng. J. AISC 2Q (1971) 55–64.
[20] J.L. Batoz, G. Dhatt, Incremental displacement algorithms for non-linear problems, Int. J. Numer. Methods Eng. 14 (1979) 1262–1267.